

Miniature Autonomous Star Tracker Based on CMOS APS

Dong Ying, You Zheng, Xing Fei, Chou Qin
 Department of Precision Instrument and Mechanics, Tsinghua University
 Beijing 100084, China; +86-10-62785802
 dongy@tsinghua.edu.cn, yz-dpi@tsinghua.edu.cn,
 xingf02@mails.tsinghua.edu.cn, qzzh00@163.com

ABSTRACT: An APS (Active Pixel Sensor) based autonomous star tracker (AASST) has been proposed for small satellite and microsatellite attitude determination. A prototype of AASST has been developed. It has low mass of 1kg, low power of 3W, high rate up to 5Hz, and acquisition success rate of higher than 99.9%. The improvements in dimensions and performances are realized with the replacement of the CCD (Charge Coupled Device) by the APS. The optical design of the prototype is based on PSF (Point Spread Function) which is more adaptive for star tracker's operation than the traditional MTF (Modulation Transfer Function) criterion and can greatly reduce the difficulty of wide field of view aberration balance. The autonomous processing electronics is based on APS-FPGA-DSP flow operation which contributes mostly to the achievements of high integration and high rate. A new method is proposed for the star tracker performances testing, especially for the validation of Lost-In-Space star identification and attitude determination algorithms. In this paper, the optical design tradeoffs, the electrical modularization strategy and the star tracker testing method are introduced. The performances of the AASST prototype have been verified through real night sky experiments.

INTRODUCTION

Modern star trackers can achieve the highest accuracy among spacecraft attitude determination devices¹. The early star trackers were based on vacuum tube, which limited the accuracy and stability improvement of the instruments. The second generation of star tracker used CID (Charge Injection Device) or CCD as detector. The instrument performances have been greatly improved. As the rapid development of IC (Integrated Circuit) technology, a new generation of star tracker has come into being. They are the so-called autonomous star trackers. Autonomous star trackers are equipped with micro-processor and memory, can provide attitude information directly². Nowadays CCD based autonomous star trackers have developed into a number of commercial types. Commercial star trackers typically have mass of ~3kg, power consumption of ~10W, update rate of ~10Hz, average accuracy of 10" (pitch/yaw) and 40" (roll)^{3, 4, 5, 6, 7}. Besides the consistent pursuance of low mass and power, high accuracy and rate, efforts have been made for star trackers to improve the reliability of all sky autonomous star identification.

However, it is predicted that APS will replace CCD used in the next generation of star tracker⁸. APS is manufactured using CMOS (Complementary Metal Oxide Semiconductor Transistor) technology, which provides the detector with high functional integration and low power consumption. Since the whole read-out and sampling electronics is placed on the detector chip, the area of printed circuit board is saved and the parts count for a star tracker is reduced

accordingly. Along with that, the unit mass and costs are reduced. Therefore the replacement of CCD by APS enables the construction of small, power saving and inexpensive star trackers for future space missions.

APS star trackers are still in prototype phase. JPL has proposed an ultra-low power (70 mW), ultra-low mass (42 grams), high accuracy (7.2") and very fast (50 Hz) Micro APS based Star Tracker (MAST). The MAST consists of only two chips: a CMOS APS image detector optimized for star tracker applications and an ASIC (Application Specific Integrated Circuit) chip including I²C (Inter-IC) interface, memory and an 8051 MCU (Microprogrammed Control Unit). MAST outputs raw pixel data from small windows and puts most of the computational burden on the spacecraft computer^{9, 10}.

We have proposed an APS based Autonomous Star Tracker (AASST) and a brightness independent star identification algorithm for Lost-In-Space 3-axis attitude acquisition^{11, 12}. The star tracker prototype has been developed. It contains inside memory and microprocessor, performs all functions by itself and outputs quaternion directly. In the following sections, design concept and a test method of AASST prototype will be introduced.

OPTICS

The main task of the star tracker optics is not to clearly image the stars, but to accurately locate the stars. So if we can properly defocus the optics to spread each star spot onto several pixels, some interpolation algorithms can be used to centroid the

star spots with subpixel accuracy. The energy distribution of the spot is the Point Spread Function (PSF). Then the optical design of star tracker is to optimize the PSF for the application of subpixel techniques, instead of balancing the aberrations.

Figure 1 shows the sketch of the AAST optics, which is composed of a quartz protection window in the front, 7 spherical lenses and a detector window. Table 1 gives the key parameters of the AAST optics. The main image qualities to be considered in the optical design of the AAST prototype include the spot diagram, energy convergence, chromatism and distortion.

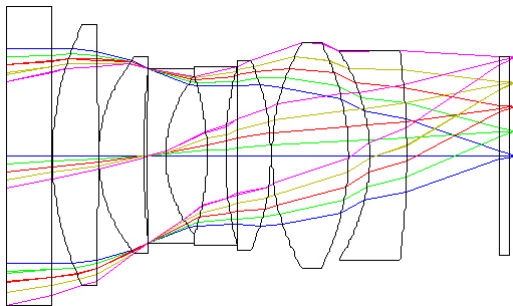


Fig. 1 Sketch of AAST optics

Table 1 Key parameters of AAST optics

Parameter	Value
Wavelength range	500~800nm
Focal length	35mm
F/#	F/1.52
Field of view	34°(circumcircle) 24.5°(inscribed circle)
Pixel size	15×15μm
Spot size	3×3 pixels
Optical transmission	75%

Spot Diagram

Figure 2 shows the chromatic spot diagrams in five half fields of view: 0°, 4.25°, 8.5°, 12.75°, 17°. It can be seen that all the spots are near round in shape. Although departure of the spots shape from round increases as the spots apart from the center of the field of view, the symmetry feature of the monochromatic spots is strictly kept even in the edge of the field of view. Spots shape, especially the symmetry feature is essential for the star tracker to achieve high accuracy by utilizing subpixel centroiding techniques.

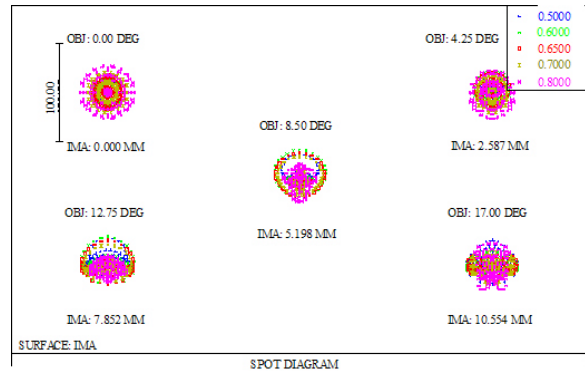


Fig. 2 Spot diagrams of AAST optics

Energy Convergence

Figure 3 shows the spots energy distribution of the AAST optics. The abscissa represents the distance from the spots center and the ordinate represents the proportion of energy that converges in the circle with the radius equal to the distance. It can be seen from the figure that in 3×3 pixels, i.e. in the circle range of 22.5μm radius, energy convergence proportion of 0°, 4.25°, 8.5°, 12.75° and 17° half fields of view are respectively 0.886, 0.928, 0.972, 0.856 and 0.864, which means that more than 85% energy is converged in 3×3 pixels.

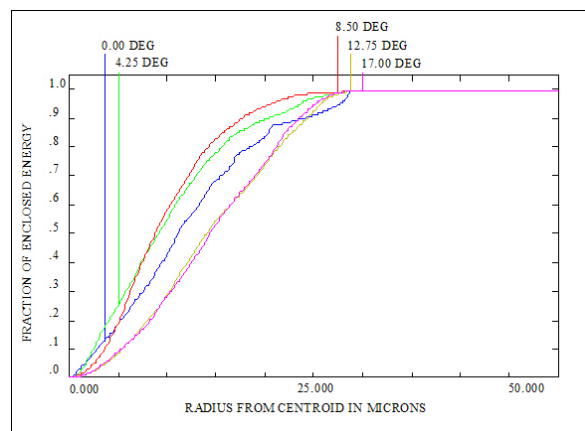


Fig. 3 Spots energy distribution of AAST optics

Chromatism and Distortion

Select three wavelength bands: 500 nm ~600 nm, 600 nm ~700 nm and 700 nm ~800nm, with 550 nm, 650 nm and 750nm (the center wavelength of each band) as the reference wavelength for each band, the chromatic aberration rms of each band is lower than ±1μm. The maximum value of the distortion is -0.99 % , and the distortion does not change with wavelength. That means the optics has not chromatic distortion.

ELECTRONICS

The electronics of the AAST prototype is provided with ten function modules:

- 1: APS readout module
- 2: Image filter and process module
- 3: Threshold segmentation and process module
- 4: Efficient data storage module
- 5: Star spots data reconstruction module
- 6: Star spots centroiding module
- 7: Star pattern recognition module
- 8: Attitude calculation module
- 9: Host-computer communication module
- 10: Catalog and database load module

There modules 1, 2, 3 and 4 are performed by FPGA (Field Programmable Gate Array), modules 5, 6, 7 and 8 are performed by DSP (Digital Signal Processing) and module 9 is performed by MCU. Module 10 is performed by FPGA and DSP together. The data communication between FPGA and DSP, DSP and MCU are all through DPRAM (Dual Port Random Access Memory). FLASH and SBSRAM (Synchronous Burst Static RAM) are used for the storage of the reference database, processing program and some related correction data. Figure 4 gives the sketch of the AAST prototype electronics.

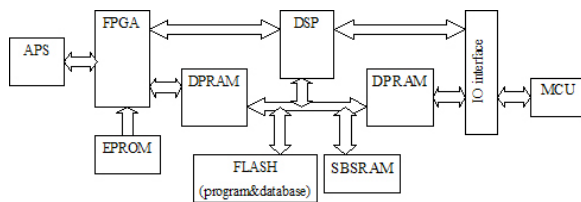


Fig. 4 Sketch of AAST electronics

The operation flow shown in figure 4 is actually for the attitude acquisition mode of the star tracker, where all the modules operate. It has been tested that the acquisition time is no longer than 1 second, and the total power is no more than 3W. In the normal mode of the star tracker, i.e. the tracking mode, the electronics can conduct sub-windowing and multi-windowing functions of the APS according to the saved pixel address of the star spots. In this way the amount of data to be transferred and stored can be greatly reduced. Besides, in tracking mode the DSP needs not to perform star identification and the whole process rate can be improved. It has been tested that the data update rate is above 5Hz and the power consumption is below 1W in the normal mode.

PROTOTYPE PACKAGE

The mechanical structure of the AAST prototype is

composed of a stray light baffle, optics housing assembly and electronics housing assembly. The dimension of the prototype is 90mm×90mm×180mm and the total mass with baffle is 1kg.

Baffle is indispensable for star trackers to be used in space. It is to shelter the lens from the on-orbit stray light. Although baffle design is an orbit, or application specific task, nowadays most commercial star trackers are equipped with standard baffles. Such baffle has certain exclusion angle of sun light and earth reflection, turning the mount of the star tracker in the spacecraft to be a specific task. We have fabricated a baffle for the AAST prototype. The exclusion angle of sun light and earth reflection are 40° and 30° respectively, and the extinction rate of the stray light is designed to be $<10^{-6}$.

The optics housing assembly and the electronics housing assembly respectively support the lens and the electronics of the AAST prototype. Design of the housing assembly is on the promise that the application requirements of the lens and the electronics are satisfied, and takes into consideration of the mass budget, operating temperature, space radiation and vacuum conditions. Figure 5 shows the package of the star tracker prototype.

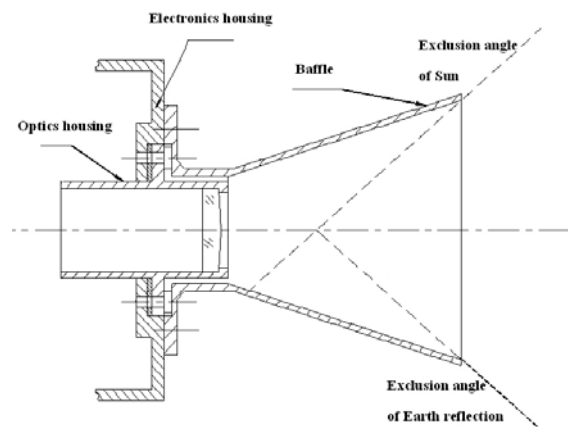


Fig. 5 Package of AAST prototype

REAL NIGHT SKY TESTS

Real night sky observation is the optimal method for star tracker calibration and test. In this method star tracker is fixed on an astronomical telescope mount with its boresight aligned with the axis of the telescope. JPL, for example, tests the hardware and software performances of the developed star trackers in this way¹³.

The employment of astronomical telescope is too expensive for us, especially in the development phase of a star tracker. However, Earth is an available at all

time and high precise rotating platform that can be used by anyone with no cost. We have proposed a novel method for star tracker performances test where expensive astronomical telescope can be replaced by the earth. This method has been proved feasible, especially to the validation of the lost-in-space star identification algorithm.

Figure 6 shows the system set-up. The star tracker is mounted on a tripod which is firmly fixed on the flat ground. The boresight of the star tracker is pointed to the zenith where atmosphere perturbation is considered minimum. Since real night sky observation must be performed in the absence of ambient lights, we carried out all the experiments at an observation station of the National Astronomical Observatories, on 4 September, 2005 when the moon is just new. The hardware performance of the APS star tracker was tested on the whole using a number of images of sky area near Polaris with 0.01s, 0.1s, 0.2s, 0.4s, 1s exposure time. Star with 4.65Mv can be sensed with 200ms exposure. So it can be presumed that the anticipant 5Mv magnitude sensitivity could be achieved when the star tracker operates in the earth orbit.

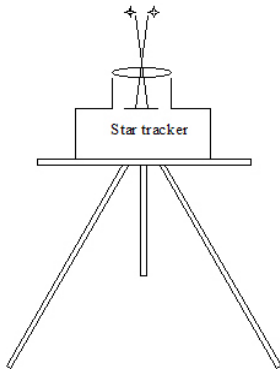


Fig. 6 Real night sky experiment system configuration

Since the star tracker is fixed on the earth, it can be considered having a rotation attitude movement along with the earth. Testing this attitude movement and referring it to the earth rotation the software performance can be tested.

There are three coordinate systems involved in the following analysis: the Celestial Reference Frame (CRF), the Terrestrial Reference Frame (TRF) and the Star Tracker Coordinate Frame (SCF)¹⁴.

The CRF is a non-rotating coordinate frame defined by celestial objects. It is the inertial reference system. The simplified description of the CRF is: the Z axis is toward the Earth's north pole, the X axis is to the vernal equinox direction, and the Y axis completes the proper orthogonal system. The TRF is an

Earth-fixed coordinate frame. The axis definition is the same as that of the CRT, and they have the common origin at the earth center. The difference between the TRF and CRF is that the TRF is rotating together with Earth. The SCF is the coordinate frame fixed to the star tracker. The origin is at the center of the detector, and the X and Y axis are parallel to the detector row and column direction respectively. The Z axis meets the right hand regularity with the X and Y axis. Figure 7 shows the definition of the three coordinate systems.

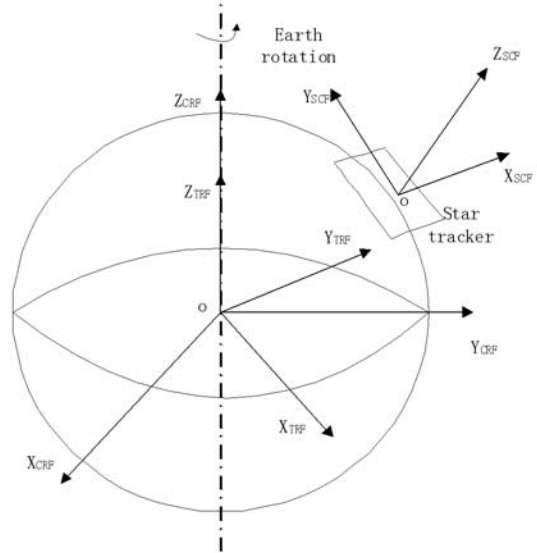


Fig. 7 Definition of the CRF, TRF and SCF coordinate systems

Since the star tracker is fixed on the earth, the relationship of the SCF and the TRF is fixed, i.e.

$$\begin{bmatrix} x \\ y \\ z \end{bmatrix}_{SCF} = A_{S-T} \begin{bmatrix} x \\ y \\ z \end{bmatrix}_{TRF} \quad (1)$$

Where the transform matrix A_{S-T} is determined by the star tracker boresight direction in the TRF. According to the Euler angle rotation as 3-1-2, the A_{S-T} can be written as:

$$A_{S-T} = \begin{bmatrix} C\psi C\phi - S\psi S\theta S\phi & C\psi S\phi + S\psi S\theta C\phi & -S\psi C\theta \\ -C\theta S\phi & C\theta C\phi & S\theta \\ S\psi C\phi + C\psi S\theta S\phi & S\psi S\phi - C\psi S\theta C\phi & C\psi C\theta \end{bmatrix} \quad (2)$$

where

$$C = \cos, S = \sin$$

ϕ, θ, ψ respectively represent the rotation angles around the axis of $Z_{TRF}, X_{TRF}, Y_{TRF}$, and can be

calculated from equation (2):

$$\begin{aligned}\phi &= \arctan(-A_{21}/A_{22}) \\ \theta &= \arcsin(A_{23}) \\ \psi &= \arctan(-A_{13}/A_{33})\end{aligned}\quad (3)$$

where A is the abbreviation of A_{S-T} .

The TRF is rotating around the Z_{TRF} (or the Z_{CRF}), and the rotating angular rate is about 15 degrees per hour. So the transform matrix of the CRF and the TRF is as follow:

$$\begin{bmatrix} x \\ y \\ z \end{bmatrix}_{TRF} = A_{T-C} \begin{bmatrix} x \\ y \\ z \end{bmatrix}_{CRF}\quad (4)$$

$$\begin{bmatrix} x \\ y \\ z \end{bmatrix}_{SCF} = A_{S-T} \begin{bmatrix} x \\ y \\ z \end{bmatrix}_{TRF} = A_{S-T} A_{T-C} \begin{bmatrix} x \\ y \\ z \end{bmatrix}_{CRF} = A_{S-C} \begin{bmatrix} x \\ y \\ z \end{bmatrix}_{CRF}\quad (7)$$

where $A_{S-C} = A_{S-T} A_{T-C}$ is as follow:

$$A_{S-C} = \begin{bmatrix} C\psi C(\phi+\alpha) - S\psi S\theta S(\phi+\alpha) & C\psi S(\phi+\alpha) + S\psi S\theta C(\phi+\alpha) & -S\psi C\theta \\ -C\theta S(\phi+\alpha) & C\theta C(\phi+\alpha) & S\theta \\ S\psi C(\phi+\alpha) + C\psi S\theta S(\phi+\alpha) & S\psi S(\phi+\alpha) - C\psi S\theta C(\phi+\alpha) & C\psi C\theta \end{bmatrix}\quad (8)$$

Combining equation (8) with equation (3), we can get the solution of the Euler rotation angle as 3-1-2 regular:

$$\begin{aligned}\phi' &= \arctan(-A_{S-C21}/A_{S-C22}) = \phi + \alpha \\ \theta' &= \theta \\ \psi' &= \psi\end{aligned}\quad (9)$$

Then the conclusion can be drawn that the Euler rotation angle ϕ is linear increasing and θ , ψ are constant when the Euler rotation angle is calculated as 3-1-2 regular.

In the experiments, a succession of images with 200ms exposure were taken during the best period of star observation (11 pm to 1 am). Each image was processed and the centroid of the star spots in the image were determined. Then star pattern recognition was performed without prior attitude information and the 3-axis attitude of the star tracker was calculated using the identified stars. Transforming the frame from the star tracker to the inertial system, and drawing the curves of the calculated Euler rotation angles ϕ , θ and ψ with time gave the rotation track of the earth in the CRF. The experiment result is shown in figure 8.

The A_{T-C} is as follow:

$$A_{T-C} = \begin{bmatrix} C\alpha & S\alpha & 0 \\ -S\alpha & C\alpha & 0 \\ 0 & 0 & 1 \end{bmatrix}\quad (5)$$

where α is the function of time.

$$\alpha(t) = (UTS(t) - UTC) \times 15^\circ / \text{hour}\quad (6)$$

where $UTS(t)$ represents the present time of the star tracker frame, while UTC represents the Universal Time.

So the transform relationship from the CRF to the SCF is as follow:

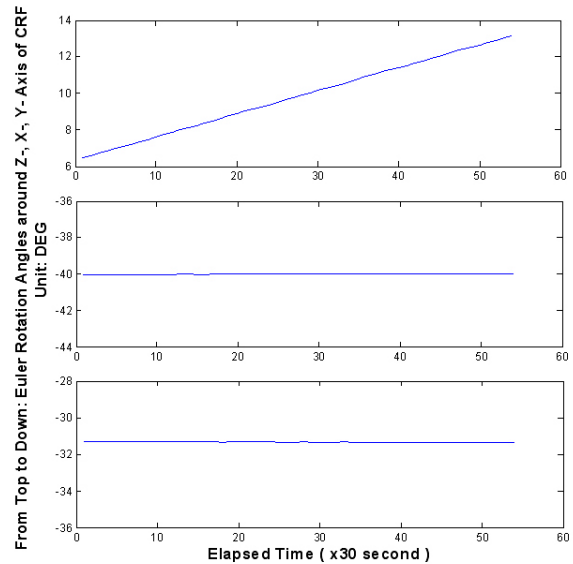


Fig. 8 Acquired Earth rotation in the CRF

The rate of ϕ is calculated to be about $15^\circ/\text{hour}$, and θ and ψ were invariable with 0.0057° and 0.0073° 1σ uncertainty respectively. The rotation is consistent with the above analysis that means no identification failure had happened, in the other word, the

Lost-In-Space star identification algorithm is feasible.

CONCLUSION

This paper reports on the development of an APS based autonomous star tracker prototype. Design trade-offs of optics, operation flow of electronics, assembly of mechanical structures are introduced. The concept of PSF based optical design, modularization strategy of electrical design, and compact package contribute to a small size, high rate, low power consumption and low cost star tracker. A new method of star tracker performances test is proposed. It uses Earth rotation as the reference instead of the expensive astronomical telescope. Real night sky experiments using this method demonstrated that the circuit quality, magnitude sensitivity, location accuracy and sky coverage of the star tracker prototype could meet the requirements of a successful operation of autonomous star tracker.

Further studies are underway to calibrate the prototype and evaluate the accuracy of the APS star tracker based on the test method proposed in this paper.

Acknowledgements

This work is partially supported by China National Research Fund for Fundamental Key Project (G2000077606). The optics of the prototype was accomplished by Institute of Modern Optical Technology, Soochow University. We are grateful to Prof. Shen Weimin and Prof. Yu Jianjun for their contribution.

References

1. Liebe, C.C., Star trackers for attitude determination, IEEE AES Magazine, vol. 10, No. 6, 1995.
2. Eisenman, A.R., Liebe, C.C. and Joergensen, J.L., The new generation of autonomous star trackers, Proceedings of SPIE, vol. 3221, 1999.
3. BALL Aerospace & Technology Corp., U.S.A., <http://www.ball.com/aerospace/ct63x.html>, 2006
4. SODERN Corp., France, <http://www.sodern.com/espace.html>, 2006
5. EMS Technologies Inc., Canada, <http://www.emsstg.com/mont/optical.asp>, 2006
6. Austrian Aerospace & TNO SPACE Holand, http://www.space.at/htmldocs/frame_m/2_1_4.html, 2006
7. Jena-Optronik GmbH, Germany, <http://www.jena-optronik.de/sensors/astro15.html>, 2006
8. Fossum, E.R., Bartman, R.K. and Eisenman, A.R., Application of the active pixel sensor concept to guidance and navigation, Proceedings of SPIE, vol. 1949, 1993.
9. Liebe, C.C., Active pixel sensor (APS) based star tracker, IEEE Proceedings, vol. 1, 1998.
10. Liebe, C.C., Dennison, E.W., Hancock, B.R., Stirbl, R.C. and Pain B., Micro APS based star tracker, Proceedings of IEEE Aerospace conference, vol. 5, 2002.
11. Ying D., Fei X. and Zheng Y., An APS based autonomous star tracker, Proceedings of SPIE, vol. 5633, 2004.
12. Ying D., Fei X. and Zheng Y., APS star sensor performance assessment through real-sky observation experiments, Proceedings of SPIE, vol. 5638, 2004.
13. Liebe, C.C., Accuracy performance of star trackers- a tutorial, IEEE Transaction on AES, vol. 38, No. 2, 2002.
14. Bae S., GLAS spacecraft attitude determination using CCD star tracker and 3-axis gyros, Doctor dissertation, University of Texas at Austin, 1998